

SPATIAL-SPECTRAL ENDMEMBER EXTRACTION FROM HYPERSPECTRAL IMAGERY USING MULTI-BAND MORPHOLOGY AND VOLUME OPTIMIZATION

Antonio Plaza, Javier Plaza and Gabriel Martin

Department of Technology of Computers and Communications
Escuela Politecnica de Caceres, University of Extremadura
Avenida de la Universidad s/n, E-10071 Caceres, Spain

ABSTRACT

We develop a new approach for characterization of mixed pixels in remotely sensed hyperspectral images. The proposed method first performs joint spatial-spectral pixel characterization via extended morphological transformations, and then automatically extracts pure spectral signatures (called *endmembers*) using volume optimization and convex geometry concepts. The proposed method outperforms other widely used approaches in the analysis of a real hyperspectral scene collected by the NASA's Airborne Visible Infra-Red Imaging Spectrometer (AVIRIS) over the Cuprite mining district in Nevada. Ground-truth information available from U.S. Geological Survey is used to substantiate our findings.

Index Terms— Hyperspectral imaging, spectral mixture analysis, endmember extraction, mathematical morphology, volume optimization

1. INTRODUCTION

The concept of hyperspectral imaging [1] originated at NASA's Jet Propulsion Laboratory in California, after the development of the Airborne Visible Infra-Red Imaging Spectrometer (AVIRIS) [2]. This system is now able to cover the wavelength region from 0.4 to 2.5 μm using more than two hundred spectral channels, at nominal spectral resolution of 10 nm. As a result, each pixel vector collected by a remotely sensed hyperspectral instrument such as AVIRIS can be seen as a *spectral signature* or *fingerprint* of the underlying materials within the pixel (see Fig. 1). An important challenge in hyperspectral image analysis is the fact that each spectral signature generally measures the response of multiple underlying materials at each site. For instance, the pixel vector labeled as "vegetation" in Fig. 1 may actually be a mixed pixel comprising a mixture of vegetation and soil, or different types of soil and vegetation canopies.

Spectral mixture analysis [3] is a popular approach to characterize mixed pixels in remotely sensed hyperspectral data sets. This approach first identifies a collection of spectrally pure constituent spectra, called endmembers in the literature, and then expresses the measured spectrum of each

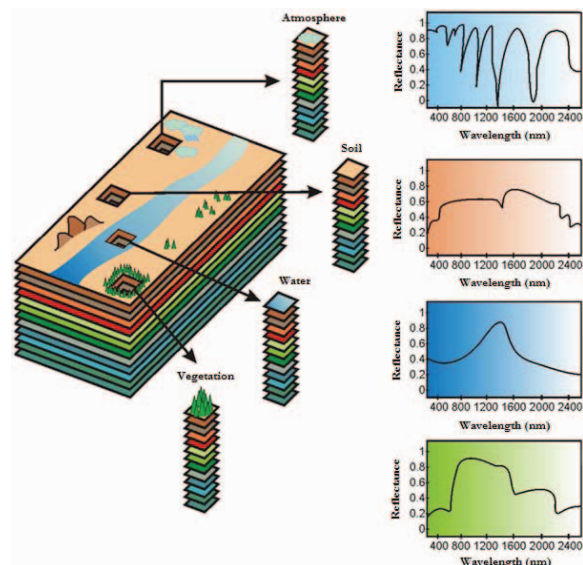


Fig. 1. The concept of hyperspectral imaging.

mixed pixel as a combination of endmembers weighted by fractions or *abundances* that indicate the proportion of each endmember present in the pixel. Over the last decade, several algorithms have been developed for automatic extraction of spectral endmembers [3]. However, most available approaches only use the spectral information contained in the image data, in spite of the fact that endmember extraction could greatly benefit from an integrated framework in which both the spectral information and the spatial arrangement of pixel vectors are taken into account.

In this paper, we develop a new approach to incorporate spatial information into the traditional spectral-based endmember search process. Specifically, we propose a hybrid algorithm which integrates multi-band mathematical morphology and volume optimization concepts. Our proposed method first quantizes the spatial and the spectral information contained in the hyperspectral data via multi-channel morphological operations. Then, a competitive endmember extraction process seeks for the simplex with maximum vol-

ume that can be formed with the sample pixel vectors in the hyperspectral image data. Due to the incorporation of spatial information, the proposed approach is able to produce endmembers with higher spatial relevance in the scene.

2. PROBLEM FORMULATION

The spectral mixture analysis problem can be formulated as follows [3]. Let us assume that a remotely sensed hyperspectral scene with n bands is denoted by \mathbf{I} , in which the pixel at the discrete spatial coordinates (i, j) of the scene is represented by an n -dimensional vector $\mathbf{X}(i, j) = [x_1(i, j), x_2(i, j), \dots, x_n(i, j)] \in \mathbb{R}^n$, where \mathbb{R} denotes the set of real numbers in which the pixel's spectral response $x_k(i, j)$ at sensor channels $k = 1, \dots, n$ is included. Under the linear mixture model assumption, each pixel vector in the scene can be modeled using the following expression:

$$\mathbf{X}(i, j) = \sum_{z=1}^p \Phi_z(i, j) \cdot \mathbf{E}_z + \mathbf{n}(i, j), \quad (1)$$

where \mathbf{E}_z denotes the spectral response of endmember z , $\Phi_z(i, j)$ is a scalar value designating the fractional abundance of the endmember z at the pixel $\mathbf{X}(i, j)$, p is the total number of endmembers, and $\mathbf{n}(i, j)$ is a noise vector. The solution of the linear spectral mixture problem described in Eq. (1) relies on the correct determination of a set $\{\mathbf{E}_z\}_{z=1}^p$ of endmembers and their correspondent abundance fractions $\{\Phi_z(i, j)\}_{z=1}^p$ at each pixel $\mathbf{X}(i, j)$. Two physical constrains are generally imposed into the model described in (1), these are the abundance non-negativity constraint (ANC), i.e., $\Phi_z(i, j) \geq 0$, and the abundance sum-to-one constraint (ASC), i.e., $\sum_{z=1}^p \Phi_z(i, j) = 1$ [4].

3. PROPOSED METHOD

In order to address the spectral mixture analysis problem, we provide a new method for spatial-spectral endmember extraction which consists of two steps: 1) morphological preprocessing, and 2) volume-based optimization. Before describing the algorithm, we introduce the approach followed to extend mathematical morphology to multi-channel images.

3.1. Multi-channel mathematical morphology

Mathematical morphology is a theory for spatial structure analysis that was established by introducing fundamental operators applied to two sets [5]. A set is processed by another one having a carefully selected shape and size, known as the structuring element (SE). Extension of the two basic operations of mathematical morphology (erosion and dilation) to multi-band data such as hyperspectral imagery with hundreds of spectral channels is not straightforward [6]. The *marginal* approach, consisting of applying mono-band morphological

operations to each channel separately and combining the results, is often unacceptable in remote sensing applications because it leads to the problem of *false colors* (in our application, this means generation of new spectral constituents).

In this paper, we adopt a vector ordering technique based on a spectral purity-based criterion [6], where each pixel vector is ordered according to its spectral angle distance (SAD) to other neighboring pixel vectors in the n -dimensional data set \mathbf{I} . Specifically, we adopt a distance-based ordering based on a cumulative distance between each pixel vector $\mathbf{X}(i, j)$ and all the pixel vectors in the spatial neighborhood given by a SE denoted by K as follows:

$$C_K(\mathbf{X}(i, j)) = \sum_{(s,t) \in K} \text{SAD}(\mathbf{X}(i, j), \mathbf{X}(n, m)), \quad (2)$$

where the SAD between the two pixel vectors $\mathbf{X}(i, j)$ and $\mathbf{X}(n, m)$ is given by:

$$\text{SAD}(\mathbf{X}(i, j), \mathbf{X}(n, m)) = \cos^{-1} \left(\frac{\mathbf{X}(i, j) \cdot \mathbf{X}(n, m)}{\|\mathbf{X}(i, j)\| \cdot \|\mathbf{X}(n, m)\|} \right). \quad (3)$$

As a result, $C_K(\mathbf{X}(i, j))$ is given by the sum of SAD scores between $\mathbf{X}(i, j)$ and every other pixel vector in the K -neighborhood. Based on the definitions above, the extended erosion $\mathbf{X} \ominus K$ consists of selecting the K -neighborhood pixel vector that produces the minimum C_K value [6]:

$$(\mathbf{X} \ominus K)(i, j) = \underset{(s,t) \in K}{\operatorname{argmin}} \{C_K(\mathbf{X}(i + s, j + t))\}. \quad (4)$$

On the other hand, the extended dilation $\mathbf{X} \oplus K$ selects the K -neighborhood pixel that produces the maximum value for C_K as follows [6]:

$$(\mathbf{X} \oplus K)(i, j) = \underset{(s,t) \in K}{\operatorname{argmax}} \{C_K(\mathbf{X}(i - s, j - t))\}. \quad (5)$$

In order to avoid changing the size and shape of the features in the image, extended morphological opening and closing operations are respectively defined as: $(\mathbf{X} \circ K)(i, j) = [(\mathbf{X} \ominus K) \oplus K](i, j)$, i.e., erosion followed by dilation, and $(\mathbf{X} \bullet K)(i, j) = [(\mathbf{X} \oplus K) \ominus K](i, j)$, i.e., vice-versa [6].

3.2. Proposed endmember extraction algorithm

3.2.1. Morphological preprocessing

In this step, sequences of extended opening by reconstruction operations [7] using SE's of varying width are constructed with the goal to capture the spatial and spectral information around each pixel vector. With this type of operators, the image features are either completely retained or completely removed in accordance with the size and shape of the structuring element [5]. The inputs to this step are an n -dimensional hyperspectral image cube, \mathbf{I} , a maximum number of iterations, t , and a structuring element K with constant size of 3×3 pixels. The output is a transformed image cube with dimensions $2t - 1$, denoted by \mathbf{I}' . The following steps are applied:

1. Compute an extended opening by reconstruction for each local pixel $\mathbf{X}(i, j)$ as follows: $(\mathbf{X} \circ K)^t(i, j) = \min_{t \leq 1} \{\delta_K^t(\mathbf{X} \circ K|\mathbf{X}(i, j))\}$, with the basic operation $\delta_K^t(\mathbf{X} \circ K|\mathbf{X}(i, j)) = \delta_B \delta_B \cdots \delta_B(\mathbf{X} \circ K|\mathbf{X}(i, j))$, i.e., δ_B is applied t times, and $\delta_B(\mathbf{X} \circ K|\mathbf{X}(i, j)) = \min\{[(\mathbf{X} \ominus K) \oplus K](i, j), \mathbf{X}(i, j)\}$.
2. Compute an extended closing by reconstruction for each local pixel $\mathbf{X}(i, j)$ as follows: $(\mathbf{X} \bullet K)^t(i, j) = \min_{t \leq 1} \{\delta_K^t(\mathbf{X} \bullet K|\mathbf{X}(i, j))\}$, with the basic operation $\delta_K^t(\mathbf{X} \bullet K|\mathbf{X}(i, j)) = \delta_B \delta_B \cdots \delta_B(\mathbf{X} \bullet K|\mathbf{X}(i, j))$, i.e., δ_B is applied t times, and $\delta_B(\mathbf{X} \bullet K|\mathbf{X}(i, j)) = \min\{[(\mathbf{X} \oplus K) \ominus K](i, j), \mathbf{X}(i, j)\}$.
3. Compute the derivative of the extended opening profile as $\mathbf{d}_i^\circ = \{\text{SAD}[(\mathbf{X} \circ K)^\lambda(i, j), (\mathbf{X} \circ K)^{\lambda-1}(i, j)]\}$, with $\lambda = \{1, 2, \dots, t\}$. The derivative of the extended closing profile is computed in similar fashion as follows: $\mathbf{d}_i^\bullet = \{\text{SAD}[(\mathbf{X} \bullet K)^\lambda(i, j), (\mathbf{X} \bullet K)^{\lambda-1}(i, j)]\}$, with $\lambda = \{1, 2, \dots, t\}$.
4. Form a $(2t - 1)$ -dimensional morphological profile for each pixel $\mathbf{X}(i, j)$ as follows: $\text{MP}(i, j) = \{\mathbf{d}_i^\circ(i, j), \mathbf{d}_i^\bullet(i, j)\}$. The resulting morphological profile is the transformed image \mathbf{I} , which can be seen as a spatial-spectral feature vector for analysis purposes.

3.2.2. Volume-based optimization

Under the linear mixing model assumption, in which the fractional abundances are subject to the ANC and ASC constraints [4], all the pixel vectors from a hyperspectral scene can be inscribed within a simplex whose vertices correspond to the spectral endmembers. Let us assume that there are p endmembers in a hyperspectral scene. If the data set contains at least $p - 1$ spectral bands, we can infer the vertices of the convex hull by calculating the simplex with maximum volume that can be formed with pixel vectors. Here, we adopt the volume-based optimization strategy used by the N-FINDR algorithm [8] for endmember extraction, but using as input the $(2t - 1)$ -dimensional morphological profile $\text{MP}(i, j)$ calculated in the morphological preprocessing step for each pixel vector $\mathbf{X}(i, j)$, instead of the pixel vector itself (i.e., we use \mathbf{I} instead of \mathbf{I}). In order to be able to work in $p - 1$ dimensions, we set $t = p/2$, where p is estimated from the original hyperspectral scene using the virtual dimensionality (VD) concept [4]. Then, the following steps are applied:

1. Let $\{\mathbf{E}_1^{(0)}, \mathbf{E}_2^{(0)}, \dots, \mathbf{E}_p^{(0)}\}$ be a set of endmembers randomly extracted from the input morphological profiles.
2. At iteration $k \geq 0$, calculate the volume defined by the current set of endmembers as follows:

$$V(\mathbf{E}_1^{(k)}, \mathbf{E}_2^{(k)}, \dots, \mathbf{E}_p^{(k)}) = \frac{\left| \det \begin{bmatrix} 1 & 1 & \cdots & 1 \\ \mathbf{E}_1^{(k)} & \mathbf{E}_2^{(k)} & \cdots & \mathbf{E}_p^{(k)} \end{bmatrix} \right|}{(p-1)!} \quad (6)$$

3. For each morphological profile $\text{MP}(i, j)$ used as input, recalculate the volume by testing the profile in all p endmember positions. If none of the p recalculated volumes is greater than $V(\mathbf{E}_1^{(k)}, \mathbf{E}_2^{(k)}, \dots, \mathbf{E}_p^{(k)})$, then no endmember is replaced. Otherwise, the combination with maximum volume is retained. Let us assume that the endmember absent in the combination resulting in the maximum volume is denoted by $\mathbf{E}_j^{(k+1)}$. In this case, a new set of endmembers is produced by letting $\mathbf{E}_j^{(k+1)} = \text{MP}(i, j)$ and $\mathbf{E}_i^{(k+1)} = \mathbf{E}_i^{(k)}$ for $i \neq j$. Step 3 is repeated for all the pixel vectors in the input data until all the pixels have been exhausted. Once a set of morphological profiles have been selected, the original pixel vectors at the spatial locations of such profiles are selected as the final p endmembers.

4. EXPERIMENTAL RESULTS

The image data set used in experiments was collected by NASA's AVIRIS system over the Cuprite mining district in Nevada¹, an area that has been extensively mapped by the U.S. Geological Survey (USGS)². The data set consists of 614×512 pixels and 224 bands in the wavelength range 0.4–2.5 μm (137 MB in size). Fig. 2(a) shows the spectral band at 587 nm wavelength of the AVIRIS Cuprite scene. The spectra of USGS ground minerals are displayed in Figs. 2(b) and 2(c). These selected spectral signatures are used in this work to assess endmember extraction accuracy.

We have conducted a cross-validation of the proposed approach with regards to other standard algorithms [3]. Three representative spatial-spectral techniques for endmember extraction in the literature are the automatic morphological endmember extraction (AMEE) algorithm [6], the spatial spectral endmember extraction (SSEE) algorithm [9], and a recently proposed spatial preprocessing (SPP) algorithm [10] which is combined in this work with the N-FINDR algorithm [8] for spectral-based endmember extraction.

Table 1 shows the SAD values between the endmembers provided by the compared methods and the corresponding USGS mineral signatures. For all considered algorithms, the input parameters have been carefully optimized in order to obtain the best possible performance with this AVIRIS scene. In order to display the results in a more effective manner, Table 1 only reports the SAD score associated to the most similar spectral endmember (out of $p = 14$ endmembers extracted by each algorithm according to the VD concept) with regards to its corresponding USGS signature. Smaller values in Table 1 indicate higher spectral similarity. As shown by the table, the proposed algorithm resulted in the largest number of minimal SAD values among all considered combinations, and also in the lowest average SAD value across the refer-

¹<http://aviris.jpl.nasa.gov/html/aviris.freedata.html>

²<http://speclab.cr.usgs.gov/spectral-lib.html>

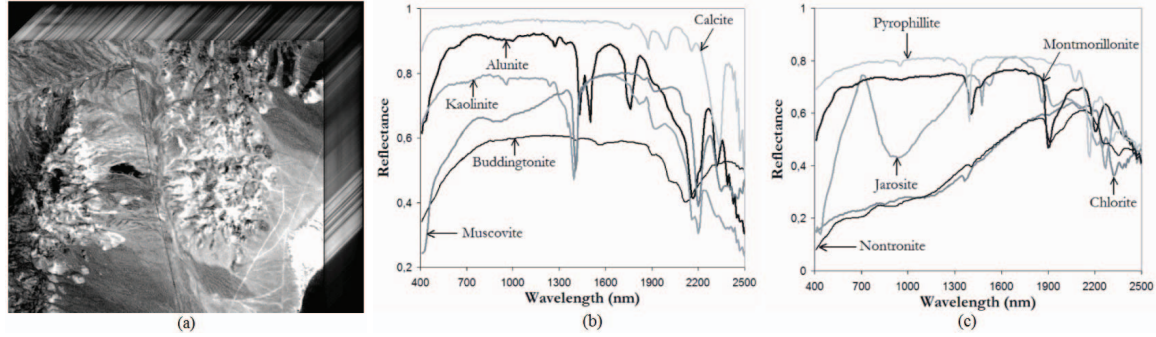


Fig. 2. (a) AVIRIS hyperspectral scene over Cuprite mining district. (b-c) Ground-truth mineral spectra provided by USGS.

Table 1. SAD-based spectral similarity scores between USGS mineral spectra and their corresponding endmembers produced by different algorithms.

Mineral signature	AMEE	SSEE	SPP	N-FINDR	Proposed
Alunite	0.084	0.084	0.109	0.174	0.084
Buddingtonite	0.073	0.072	0.145	0.134	0.073
Calcite	0.166	0.148	0.162	0.206	0.112
Kaolinite	0.152	0.194	0.138	0.229	0.136
Muscovite	0.080	0.080	0.106	0.091	0.065
Chlorite	0.093	0.102	0.108	0.135	0.081
Jarosite	0.105	0.089	0.096	0.123	0.072
Montmorillonite	0.094	0.094	0.106	0.124	0.094
Nontronite	0.102	0.099	0.099	0.119	0.089
Pyrophyllite	0.094	0.094	0.092	0.115	0.078
Average	0.104	0.105	0.116	0.145	0.088

ence USGS signatures. The other spatial-spectral algorithms (AMEE, SSEE and SPP) produced endmembers which were more similar to the reference USGS signatures than those provided by N-FINDR. This is due to the fact that geological features in the Cuprite mining district exhibit high spatial correlation. An experimental inter-comparison of the proposed method with the same algorithms using two additional hyperspectral scenes also revealed similar results (omitted here for space considerations). These results indicate that the proposed algorithm can effectively combine the spatial and the spectral information to produce higher quality endmembers.

5. CONCLUSIONS AND FUTURE RESEARCH

In this work, we have discussed the role of joint spatial-spectral information in spectral mixture analysis of hyperspectral imagery. A new algorithm for spatial-spectral endmember extraction has been proposed. The algorithm combines multi-channel mathematical morphology with volume-based optimization concepts, and compares favorably with other endmember extraction algorithms in the context of a mineral mapping application using hyperspectral data collected by NASA’s AVIRIS sensor. Further experimentation with additional scenes and endmember extraction algorithms will be conducted in future work.

6. REFERENCES

- [1] A. F. H. Goetz, G. Vane, J. E. Solomon, and B. N. Rock, “Imaging spectrometry for Earth remote sensing,” *Science*, vol. 228, pp. 1147–1153, 1985.
- [2] R. O. Green et al., “Imaging spectroscopy and the airborne visible/infrared imaging spectrometer (AVIRIS),” *Remote Sens. Environ.*, vol. 65, pp. 227–248, 1998.
- [3] A. Plaza, P. Martinez, R. Perez, and J. Plaza, “A quantitative and comparative analysis of endmember extraction algorithms from hyperspectral data,” *IEEE Trans. Geosci. Remote Sens.*, vol. 42, no. 3, pp. 650–663, 2004.
- [4] C.-I Chang, *Hyperspectral Imaging: Techniques for Spectral Detection and Classification*, Kluwer Academic/Plenum Publishers: New York, 2003.
- [5] P. Soille, *Morphological Image Analysis: Principles and Applications*, Springer: Berlin, 2003.
- [6] A. Plaza, P. Martinez, R. Perez, and J. Plaza, “Spatial/spectral endmember extraction by multidimensional morphological operations,” *IEEE Trans. Geosci. Remote Sens.*, vol. 40, no. 9, pp. 2025–2041, 2002.
- [7] M. Fauvel, J. A. Benediktsson, J. Chanussot, and J. R. Sveinsson, “Classification of hyperspectral data using SVMs and morphological profiles,” *IEEE Trans. Geosci. Remote Sens.*, vol. 42, pp. 608–619, 2008.
- [8] M. E. Winter, “N-FINDR: Algorithm for fast autonomous endmember determination in hyperspectral data,” *Proc. SPIE*, vol. 3753, pp. 266–277, 2003.
- [9] D. M. Rogge, B. Rivard, J. Zhang, A. Sanchez, J. Harris, and J. Feng, “Integration of spatial–spectral information for the improved extraction of endmembers,” *Remote Sens. Environ.*, vol. 110, no. 3, pp. 287–303, 2007.
- [10] M. Zortea and A. Plaza, “Spatial preprocessing for endmember extraction,” *IEEE Trans. Geosci. Remote Sens.*, *accepted for publication, in press*, 2009.